Two-Dimensional Soot Pyrometry with a Color Digital Camera

Blair C. Connelly, Sebastian A. Kaiser, Mitchell D. Smooke, and Marshall B. Long

Department of Mech. Eng., Yale University, New Haven, CT 06520

Abstract

The potential application of a relatively low-cost, color digital camera, for use as a three-color optical pyrometer is investigated with the goal of measuring soot temperatures within a flame. The use of the built-in color filter array (CFA) of the digital camera allows for two-dimensional imaging of flame emission at the wavelengths of the color filters. The image data provide pixel-by-pixel spectral and spatial information, which is then used to calculate the two-dimensional flame temperatures. The filter profiles of the CFA were characterized to provide a calibration for the two-color method used to calculate the temperatures. Images were taken of sooting, axisymmetric laminar ethylene flames, and the two-dimensional temperature field was calculated. Comparisons are made to temperature and soot distributions provided by a recent set of calculations. It is demonstrated that a consumer digital camera can be used effectively as a multi-wavelength pyrometer. Future work will include improved characterization of the camera and an independent direct blackbody calibration in order to provide temperatures with respect to a known reference point.

Introduction

Understanding the processes responsible for the production of soot in combustion systems is important in many aspects of combustion research. Multi-wavelength optical pyrometry is a common measurement technique used to obtain the surface temperature of soot particles and soot concentration [1 – 7]. Typically, soot emission is sampled at two or three different wavelengths using scientific charge-coupled-device (CCD) detectors and spectral filters. The use of multiple detectors makes it necessary to spatially match the images taken at the different wavelengths.

The objective of this paper is to examine the possibility of using a relatively low-cost color digital camera as an optical pyrometer. The camera's detector uses a color filter array (CFA), coated directly onto the monochrome detector, to sample red, green, and blue (RGB) signals. Ordinarily, the camera's processor recreates scenes by combining the RGB signals to determine the image color at each pixel. A demosaicing algorithm, which combines the color values at a pixel and its neighbor pixels, is used to interpolate color values from a GRGB Bayer Pattern and provide the full color at each pixel [8,9]. The maximum pixel mismatch from this interpolation is expected to be less than one pixel. Alternatively, the RGB color data can be used separately as three two-dimensional images that do not need to be spatially matched. The blackbody radiation of soot particles can be imaged at the three wavelengths of the CFA and the temperature can then be calculated using two-color ratio pyrometry. Since consumer digital cameras are not intended for use as scientific detectors, it is necessary to investigate some aspects of the data acquisition that for a scientific detector are usually manufacturer-tested and specified. The camera can then be used to image the soot emissions in flames.

Theory

The intensity of radiation, I_λ, of a particle at wavelength λ is dependent on the particle temperature T and its monochromatic emissivity ε_λ, and follows Planck's law:

$$I_\lambda(\lambda,T) = \varepsilon_\lambda \frac{2\pi hc^2}{\lambda^5\left[\exp(hc/k\lambda T)-1\right]} \tag{1}$$

where c is the speed of light, h is Planck's constant and k is the Boltzmann constant. The measured signal, S_λ, is the intensity of radiation integrated over the detection wavelengths and normalized for the detection efficiency. Following the development of multi-wavelength ratio pyrometry by Levendis et al. [2], the signal ratio at two detection wavelengths λ_1 and λ_2 is

$$\frac{S_{\lambda_1}}{S_{\lambda_2}} = C_{\lambda_1\lambda_2}\left(\frac{\varepsilon_{\lambda_1}}{\varepsilon_{\lambda_2}}\right)\left[\frac{\exp(hc/k\lambda_1 T)-1}{\exp(hc/k\lambda_2 T)-1}\right]. \tag{2}$$

The instrument constant $C_{\lambda_1\lambda_2}$ is a function of the collection efficiency of the detector, η_D, the combined lens and filter transmittance, η_L, the ratio of detection wavelengths, and the ratio of spectral bandwidths, $\Delta\lambda$, at the two detection wavelengths 1 and 2:

$$C_{\lambda_1\lambda_2} = \left(\frac{\eta_{L_1}}{\eta_{L_2}}\right)\left(\frac{\eta_{D_1}}{\eta_{D_2}}\right)\left(\frac{\lambda_2}{\lambda_1}\right)^5\left(\frac{\Delta\lambda_1}{\Delta\lambda_2}\right). \tag{3}$$

The spectral bandwidth of the filters, $\Delta\lambda$, accounts for the effects of the approximation λ = constant made when performing the spectral integration (Eq. 1 → Eq. 2), i.e., $\Delta\lambda_1$ and $\Delta\lambda_2$ are assumed to be small compared to their central

wavelength difference, $\lambda_1 - \lambda_2$. $C_{\lambda_1 \lambda_2}$ can be determined using a blackbody source of known temperature for calibration. Alternatively, the parameters (or their ratios) appearing in Eq. 3 can be measured and $C_{\lambda_1 \lambda_2}$ can then be calculated, which is the method that has been followed in this work.

Further manipulation of Eq. 2 yields the expression:

$$T = \frac{\dfrac{hc}{k}\left(\dfrac{1}{\lambda_2} - \dfrac{1}{\lambda_1}\right)}{\ln\left[\dfrac{1}{C_{\lambda_1 \lambda_2}} \dfrac{\varepsilon_{\lambda_2}}{\varepsilon_{\lambda_1}} \dfrac{S_{\lambda_1}}{S_{\lambda_2}} \left(\dfrac{1 - \exp(-hc/k\lambda_1 T)}{1 - \exp(-hc/k\lambda_2 T)}\right)\right]} . \qquad (4)$$

Assuming graybody behavior, the emissivities, ε_{λ_1} and ε_{λ_2}, cancel [4]. Since Eq. 4 is implicit in T, a solution must be determined iteratively. A starting value can be obtained using the Wien approximation to assume the temperature-dependent term, in parentheses on the right side of the equation, to be unity. Further iterations are carried out using the full formulation of Eq. 4. It is also necessary to carry out iterations of the central detection wavelengths λ_1 and λ_2. The assumption of narrowband detection filters, made to derive Eq. 2, is too restrictive for the filter characteristics of typical CFAs, because the Planck function varies significantly within the spectral detection window. As a result, when the Planck function is sampled by the CFA, the central wavelength of the detected spectral signal shifts significantly from the original central wavelength of the CFA. The result is a new effective wavelength that must be used to calculate the temperature [3, 6, 7]. This effective wavelength is inserted into Eqs. 3 and 4 for further iterations. A blackbody temperature calibration of the instrument constant would directly provide an effective $C_{\lambda_1 \lambda_2}$ as well as an effective λ_1 and λ_2, leaving only the iteration for T. The effect of wavelength shifting will be illustrated in the next section when the detector characterization is discussed.

Experiment

Normally used as a consumer product, the Nikon D70 single lens reflex (SLR) digital camera has been used here as a multi-wavelength optical pyrometer. The D70 was chosen because it offered the necessary manual user control of settings at a reasonable price. The CCD detector is 23.7 mm by 15.6 mm and has 6.1 million (effective) pixels (2012 x 3038). Data were taken using the Nikon Capture Control software to operate the camera remotely and to transfer the images to a computer. All image enhancement options, such as sharpness, contrast, color, and saturation, were set to either "normal" or "none", as applicable, in order to ensure shot-to-shot consistency. A white balance of "direct sunlight", with a color temperature of 5200 K, was selected. Once chosen, the same settings were used for all data acquisition.

Files were saved in the camera's "NEF" format, which is Nikon's 12-bit lossless compressed "RAW" format. Although used by many camera manufacturers as a designation for unprocessed images, "RAW" is not a standardized format (unlike TIF, JPG, etc.). Consequently, some careful examination of the resulting image is necessary to ensure consistent reconstruction of the underlying intensity data. To facilitate a more transparent analysis, the open-source image-processing software OMA [10] was modified to be able to import and appropriately display this Nikon-specific data format. Suitable ANSI C-code was adapted from a publicly available software library on the World-Wide Web [11].
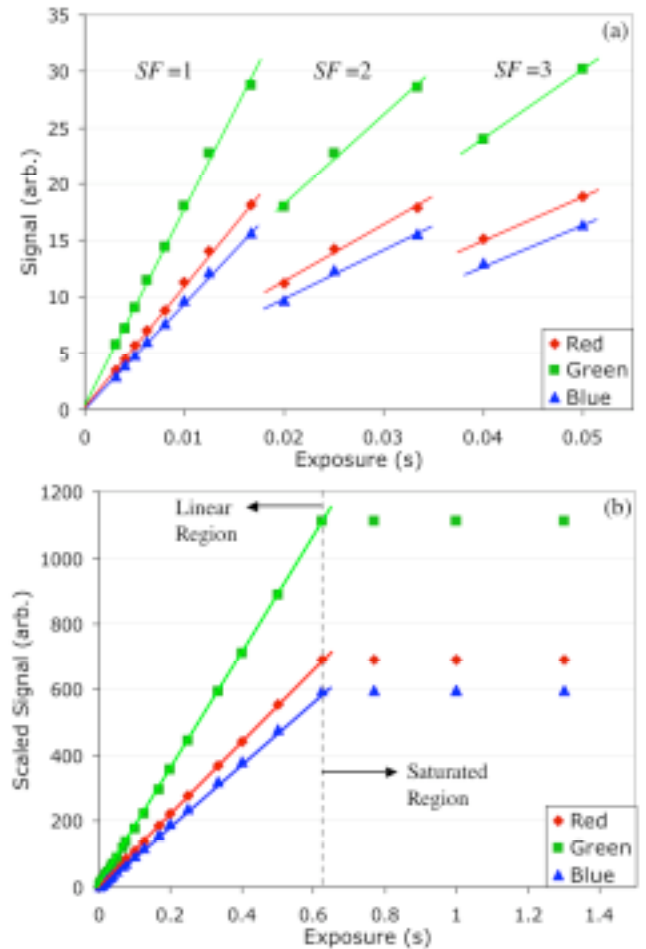
Fig. 1: Signals from the three color channels as a function of camera exposure. Data correspond to a central position of the sooty portion of a 40% ethylene flame. (a) Measured signal vs. exposure time. Note the different slopes among groups of data points, (b) scaled data using the scale factors denoted in (a). Note that the axes of (b) span a much wider range of exposures and signals than those of (a).

As a first step, the performance of the D70 under controlled conditions was investigated. It was verified that the detector signal in all three channels decreases linearly with attenuation and increases linearly with exposure, up to the point where the channels saturate. Fig. 1 demonstrates

this linearity of signal as a function of exposure using a region with significant soot incandescence in an ethylene flame as the light source. A colored glass filter was also used as discussed below. Fig. 1a displays the acquired signal as a function of exposure time. In this plot, groups of points can be discerned. The camera's pre-processor has apparently applied a different scale factor to these groupings before outputting the data. A line through the origin can be fit to the data points in each group with the slope of the linear fit being inversely proportional to the scale factor. In Fig. 1a the scale factors SF are shown above their respective group. Fig 1b shows that indeed multiplying the data in each group with the corresponding scale factor yields a signal linearly increasing as a function of exposure time across all groups and for all three channels. As would be expected from a CCD-detector, each channel saturates at some level and further increase of exposure time yields no increase in signal. Within the linear region, the signal ratio between the different color channels exhibits a standard deviation of 1% across all data triplets. In the following, the camera was operated in this linear regime, ensuring proportionality of the channels for a given spectral signal.

The next step was the characterization of the detector's spectral response, presumably mostly determined by the CFA. Images were taken of a uniformly lit white background with a selection of 10 nm bandwidth interference filters spaced in central wavelengths to cover the visible spectrum. The signal was then normalized for the spectral variation of the light source using the known response of a photodiode, through the same collection optics and geometry. The red, green, and blue filter profiles of the CFA appeared to be approximated well by Gaussian functions with central wavelengths of 620, 545, and 475 nm, respectively, each with a standard deviation of 40 nm. The uncertainty in the measured central wavelengths was estimated to be 5 nm. Plots displaying these fitted filter profiles are shown in Fig. 2a. The peak transmission of each filter profile was assumed equivalent, as the data did not provide enough information to specify different transmissions. This assumption will require further investigation in the future when characterization of the CFA will be revisited.

The emitted blackbody signal of soot particles at typical flame temperatures (1800 - 2000 K) decreases very rapidly in the visible region from red to blue. A BG 13 colored-glass filter was placed in front of the camera, in order to achieve a better match in signal magnitudes across the three channels and hence make better use of the dynamic range of the detector. Fig. 2a also shows the transmission function of the colored-glass filter. The resulting effective transmission for the three channels after the addition of the BG 13 filter is shown in Fig. 2b. The variation in throughput across the channels now should balance the variation in input from the Planck emission spectrum, shown here for a nominal temperature of 1900 K. In addition to the changes in overall transmissions, it can be seen that the red, green, and blue
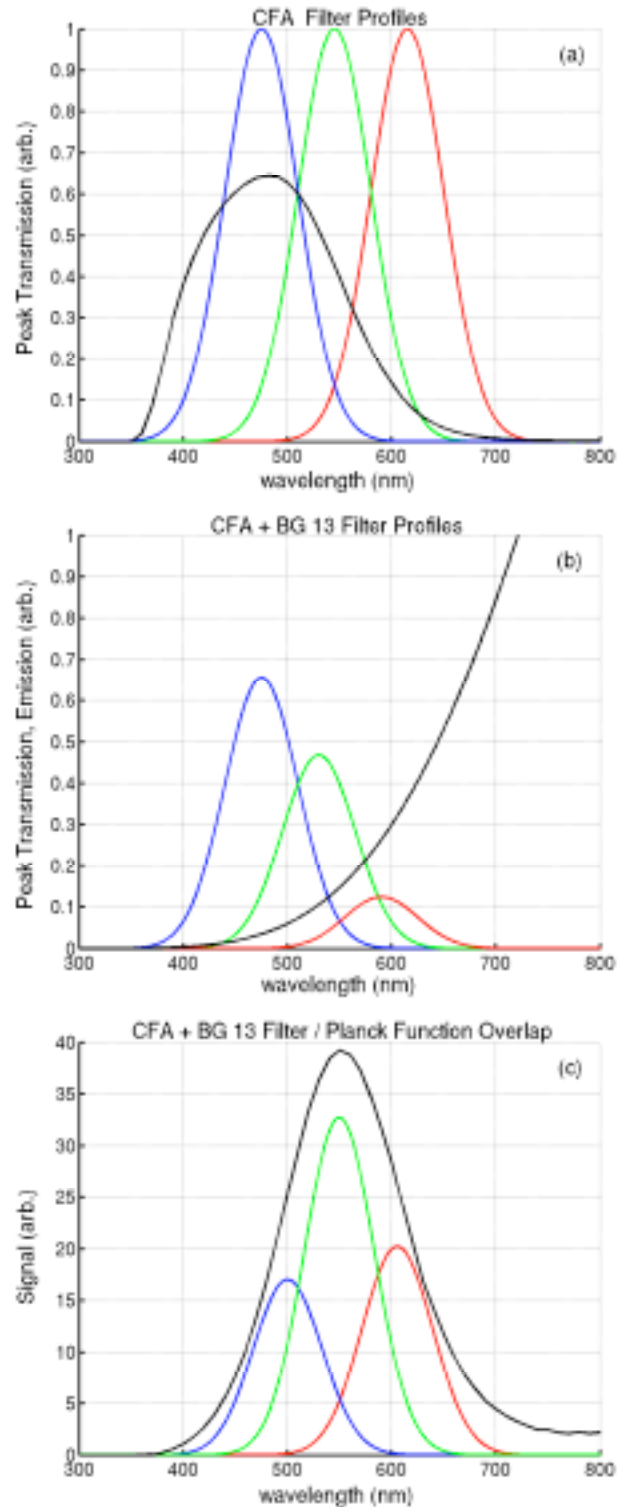
Fig. 2 : Filter functions of the red, green, and blue channels of the camera, colored accordingly. (a) Fitted filter functions of the camera CFA and measured transmittance of a Schott BG 13 colored-glass filter (black line), (b) effective filter functions when used with the BG 13 filter placed in front of the camera lens and Planck emission spectrum for a black body at 1900 K (black line), (c) spectral overlap of the effective filter functions and emission spectrum from (b) as well as the BG 13-filtered Planck spectrum (black line). Note the red-shift of the central wavelengths.

central wavelengths are blue-shifted and are now 590, 530, and 475 nm, respectively. Fig. 2c shows the expected spectral signal for each channel when observing soot particles at flame temperatures as well as the Planck spectrum filtered by the BG 13. There are two features worth noting in this plot: the maximum signals across all three channels are reasonably equalized, and the central wavelengths have been red-shifted. The new effective wavelengths of the detected spectrum are now approximately 605, 550, and 500 nm for the red, green, and blue channels, respectively. The shifts are due to the significant variation of the unfiltered Planck spectrum within the range of wavelengths covered by each channel. It is for this reason that the algorithm used to calculate the temperature iterates the detector's central wavelengths along with the calculated temperature.

Following this preliminary detector characterization, data were taken in sooting, axisymmetric laminar ethylene flames, with varying degrees of fuel-dilution. Details on the burner configuration have been previously reported in Refs. 12 and 13. Briefly, a central jet 4 mm in diameter is surrounded by a coflow of 50 mm diameter. Nominal fuel and coflow velocities were matched at 35 cm/s. Images were taken of the soot radiation at ethylene concentrations of 32%, 40%, 60%, and 80% (by volume). The flames were imaged at f/16 through an 85 mm focal length lens for the 32%, 40%, and 60% cases, and at f/20 through a 70 mm focal length lens for the 80% case. Because the flames are axisymmetric, an Abel inversion can be used to reconstruct the two-dimensional radial profile of soot emission. The lens configuration was chosen to approximate parallel ray collection, which is a necessary assumption of an Abel inversion [14, 15]. The resulting temperature calculations for the cases of 40% and 60% ethylene are compared with the corresponding results of recent numerical work on sooting laminar ethylene flames [13].

Our model of an axisymmetric laminar diffusion flame considers an unconfined laminar flame in which a cylindrical fuel stream is surrounded by a coflowing oxidizer jet. Computationally, we utilize a velocity-vorticity approximation in which the elliptic two-dimensional governing equations are discretized on a two-dimensional mesh. The resulting nonlinear equations are then solved by a combination of time integration and Newton's method. The Newton equations are solved by a preconditioned Bi-CGSTAB iteration. We determine the grid points of the two-dimensional mesh by equidistributing positive weight functions over mesh intervals in both the r and z directions. The size of the time steps is chosen by monitoring the local truncation error of the time discretization process (see also, Ref. [16]). The binary diffusion coefficients, the viscosity, the thermal conductivity of the mixture, the chemical production rates as well as the thermodynamic quantities are evaluated using vectorized and highly optimized transport and chemistry libraries [17].

Results and Discussion

Comparison of the experimental temperature field from a 40% ethylene flame to the numerically calculated temperature is shown in Fig. 3, while Fig. 4 displays the same for a 60% ethylene flame. The experimental data are noisy in the vicinity of the centerline, particularly at the higher ethylene concentrations. For the purpose of processing, flame images were divided along the centerline before performing an Abel inversion. The noise on the centerline of the experimental images appeared as a result of the inversion process. A low magnitude noise from the centerline to the peak of the distribution is an artifact of all Abel inversion algorithms [14]. This effect becomes more noticeable as the concentration of ethylene increases because the soot is redistributed from the center of the flame towards the edges. The experimental temperature field could only be measured where the flame contains soot. Therefore, the dark blue region in the figures does not necessarily indicate low temperatures, but rather the absence of a sufficient amount of soot to obtain temperature information. The numerical model calculates the temperature over the entire space, not just in sooting regions. For an easier comparison, the model's data have been filtered by a mask corresponding to locations of significant amounts of soot, as calculated by the model. As a first approximation, an average sized soot class was used to create the mask.
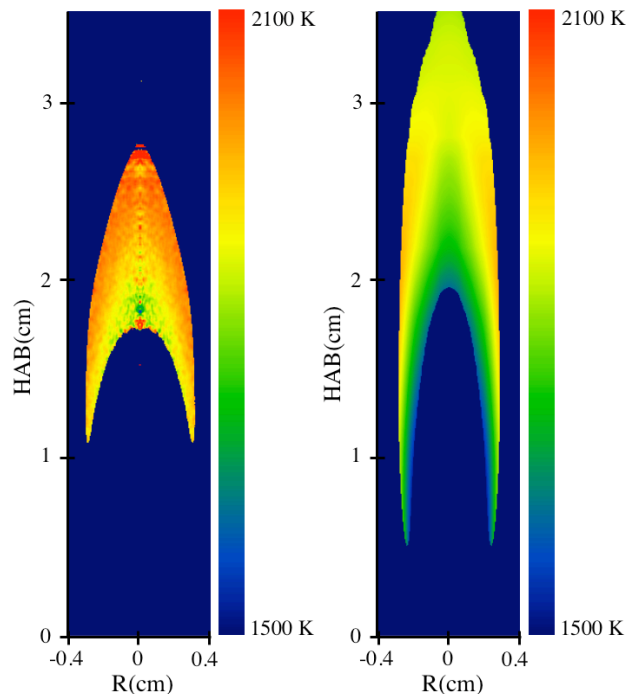
Fig. 3: Experimental (left) and numerically calculated flame temperatures (right) for a 40% ethylene flame. Both images are on the same spatial and temperature scale.

In Figs. 3 and 4, the temperature scale is kept constant between the experimental and numerical images. Overall, the experimental temperatures are about 75 to 150 K higher than the numerically calculated ones, primarily in the middle sections of the flame. Without a known temperature

calibration for reference in the experiment, it is difficult to judge whether the experiment is calibrated too high, or whether the model's temperatures are calculated to low. It was found through simulations that a 5 nm change in any one channel's central wavelength corresponds to a shift of about 70 K in the calculated temperature. The temperature calculation is also sensitive to variations in the peak transmittance of the effective CFA, particularly for the red channel since addition of the BG 13 filter lowers its peak transmittance to only 12%. Since a two-color method is used to calculate temperatures, there exists a redundancy between the three possible two-color combinations. An indication that the CFA characterization was fairly successful is that these three temperature fields typically agree within 30 to 60 K. The experimental temperature results shown each are the averages of the different color combinations.
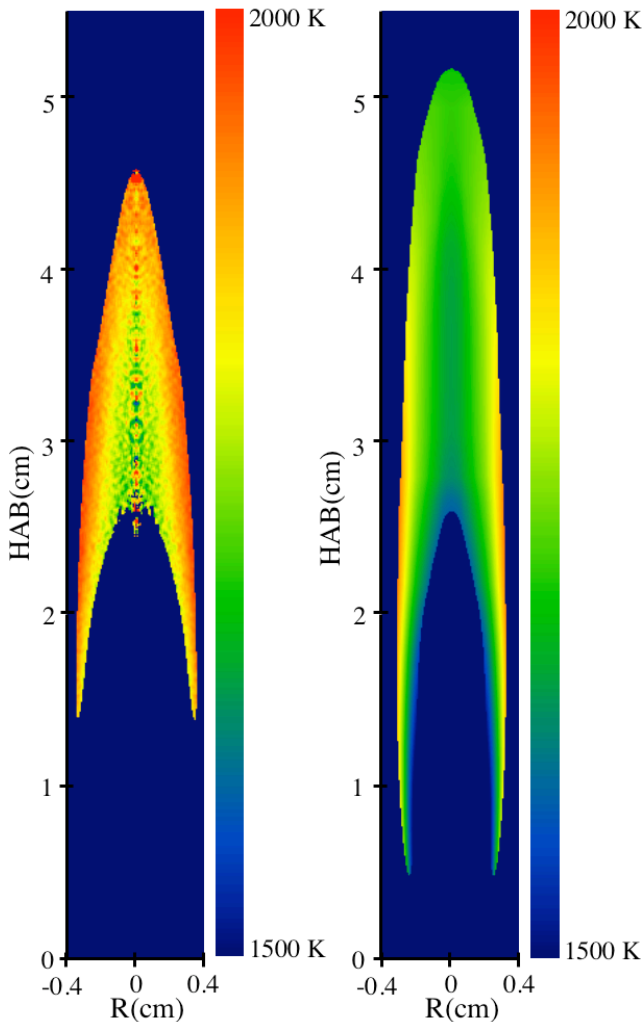
Fig. 4: *Idem* for a 60% ethylene flame.

Even though a direct temperature calibration is not available at present, some comparisons of experimental and numerical results can be made. The overall decrease in temperature for flames with more soot is seen in both experimental and numerical results. Consistent with previous comparisons between measured and calculated soot distributions [13], the model predicts soot over a somewhat larger region than is experimentally observed. Both computation and experiment show that the temperatures rise toward the edge of the soot-containing regions, particularly away from the centerline. The largest departure in the qualitative behavior between measured and calculated soot temperatures occurs near the top of the soot cone. The measurements show the high temperatures at the edge of the soot-containing region continuing to the tip, whereas the computations predict a lower temperature on the centerline as compared to the edges.
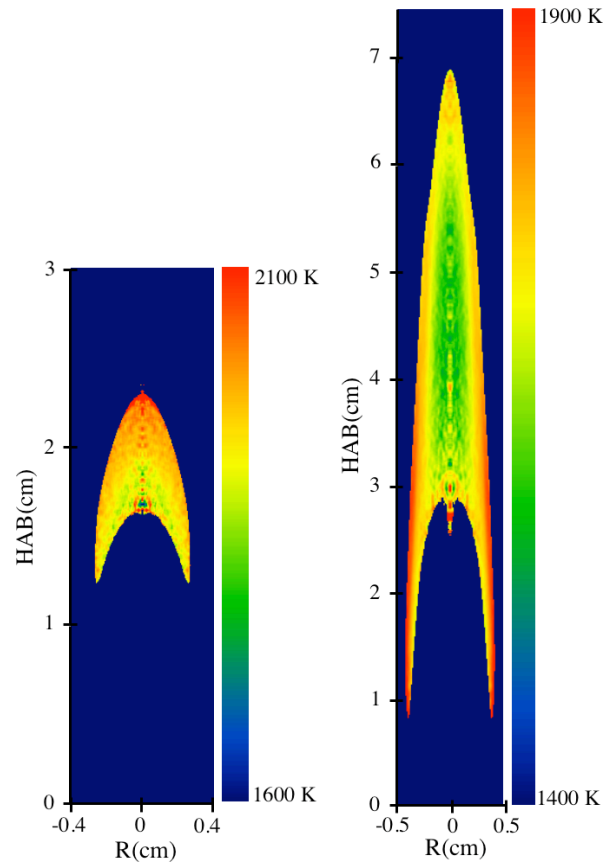
Fig. 5: Experimental flame temperatures for a 32% ethylene flame (left) and for an 80% ethylene flame (right). Note that both spatial and temperature scales are different for each image.

Data taken for 32% and 80% ethylene flames are displayed in Fig. 5. Note that the two images are shown on different temperature and spatial scales. No numerical results are available for comparison to these images at this time. Because the soot in the 80% flame is primarily distributed along the edges of the flame, the signal there is significantly higher. As a result, it was necessary to average a number of shots in order to obtain sufficient signal levels in the center of the flame without saturating the detector at the flame edges. The edge-heavy soot distribution also created more noticeable artifacts from the Abel inversion in the central region of the flame. The "tail" that dips down in

the center of the temperature field is due to signal ratios of noisy data, and is not indicative of the actual temperature.

With a set of experimental temperature values for four different fuel concentrations, some comments can be made about trends in the temperature fields. As noted previously, the lower-concentration flames tend to have higher peak temperatures, with their highest temperatures located more towards the top of the soot cone. The higher-concentration flames tend to have lower peak temperatures, with their highest temperatures located along the edges of the flame. If these temperature fields were compared to images displaying soot concentration, a correlation between the higher temperatures and soot location should be visible. The lower-concentration flames have most of their soot near the centerline, while the higher-concentration flames have more soot along their edges.

Conclusions

The Nikon D70 consumer digital camera was examined as a practical, low-cost alternative to scientific CCD cameras, for use as an optical pyrometer. It was verified that the D70 could be operated with settings that provided a linear response to a constant signal, and signal values were consistent from shot to shot. Initial tests of the validity of using a consumer digital camera as a pyrometer were promising, as reasonable temperature measurements were obtained from axisymmetric laminar ethylene flames. Comparisons were made with a numerical model that calculates the soot and temperature field. The experimental temperatures were consistently higher than the model's, and showed a different distribution of the high temperatures along the centerline. More precise conclusions will depend on better camera calibration.

Future work in the development of the camera as a pyrometer primarily involves improving the detector characterization. Since it was shown that the temperature calculation is quite sensitive to the filter profiles of the CFA, better characterization of the CFA will be required. While exposing the camera with different interference filters in front of the lens was a sufficient method to gain a general idea of the filter profiles, more narrowband measurements of better-controlled intensity should give more highly resolved data points and more precise values for the filter transmission. The potential use of a white light source and a monochromptor is being investigated for this purpose. Independently, direct calibration of the camera with a blackbody source of known, variable temperature should be performed. This method would allow for the calibration constant and filter wavelengths used in the temperature calculation to be adjusted with respect to a known reference point. Once properly characterized, this pyrometric method will be used for further comparisons to computed temperature fields in the ethylene flames described above. The use of a direct temperature calibration will also make it feasible to calculate the soot volume fraction using the temperature field [3,5].

References

1. Snelling, D.R., Thomson, K.A., Smallwood, G.J., Gülder, O.L., Weckman, E.J., and Fraser, R.A., *AIAA Journal* **40**: 1789-1795 (2002)
2. Levendis, Y.A., Estrada, R.E., and Hottel, H.C., *Review of Scientific Instruments* **63**: 3608-3622 (1992)
3. Cignoli F., De Iuliis, S., Manta, V., and Zizak, G., *Applied Optics* **40**: 5370-5378 (2001)
4. Panagiotou, T., Levendis, Y., and Delichatsios, M., *Combustion and Flame* **104**: 272-287 (1996)
5. Zhao, H., and Ladommatos, N., *Progress in Energy and Combustion Science* **24**: 221-225 (1998)
6. Boslough, M.B., and Ahrens, T.J., *Review of Scientific Instruments* **60**: 3711-3716 (1989)
7. Anselmi-Tamburini, U., Campari, G., Spinolo, G., and Lupotto, P., *Review of Scientific Instruments* **66**: 5006-5014 (1995)
8. Bayer, B.E., *U.S Patent 391065* (1976)
9. Chang, L.L., Tan, Y.P., *IEEE Transactions on Consumer Electronics* **50**: 355-365 (2004)
10. Kalt, P.A., Long, M.B., www.oma-x.org (accessed 01/2005) – includes the RAW import routines implemented for this work
11. Coffin, D., www.cybercom.net/~dcoffin/dcraw/ (accessed 01/2005)
12. McEnally, C.S., Schaffer, A.M., Long, M.B., Pfefferle, L.D., Smooke, M.D., Colket, M.B., and Hall, R.J., *Proceedings of the Combustion Institute* **27**: 1497-1505 (1998)
13. Smooke, M.D., Hall, R.J., Colket, M.B., Fielding, J., Long, M.B., McEnally, C.S., Pfefferle, L.D., *Combustion Theory and Modelling* **8**: 593-606 (2004)
14. Walsh, K.T., Fielding, J., and Long, M.B., *Optics Letters* **25**: 457-459 (2000)
15. Dasch, C.J., *Applied Optics* **31:** 1146-1152 (1992)
16. Smooke, M.D, Xu, Y., Zurn, R., Lin, P., Frank, J., and Long, M.B., *Proceedings of the Combustion Institute* **24**: 813-821 (1992)
17. Giovangigli, V., and Darabiha, N., in: Brauner, C., and Schmidt-Laine, C. (Eds.), *Mathematical Modeling in Combustion and Related Topics*, Martinus Nijhoff, Dordrecht, NATO Advanced Scientific Instruments Ser. E, Vol. 140, p. 491 (1987)